Journal of Fluorine Chemistry 130 (2009) 742–748

Contents lists available at ScienceDirect

Journal of Fluorine Chemistry

journal homepage: www.elsevier.com/locate/fluor

Shape-selected synthesis, characterization and optical properties of $KMnF_3$ micropolyhedra, microspheres and hollow microspheres

Jie Sheng [a,b], Kaibin Tang [a,b,*], Dong Su [b], Suyuan Zeng [a,b], Yunxia Qi [a,b], Huagui Zheng [b]

[a] Division of Nanomaterials and Nanochemistry, Hefei National Laboratory for Physical Sciences at the Microscale, Hefei, Anhui 230026, PR China
[b] Department of Chemistry, University of Science and Technology of China, Hefei 230026, PR China

ARTICLE INFO

Article history:
Received 30 March 2009
Received in revised form 16 May 2009
Accepted 28 May 2009
Available online 30 June 2009

Keywords:
Crystal morphology
Hydrothermal synthesis
Fluoride
Perovskites
Photoluminescence

ABSTRACT

Micropolyhedra, microspheres and hollow microspheres of the cubic $KMnF_3$ were selectively prepared by controllable, hydrothermal method at 120 °C. Manganese acetate and potassium fluoride were employed as the starting materials in the reaction, and variety of polyethylene glycol and dosage of citric acid were demonstrated to be responsible for the shape evolution. The samples were characterized by X-ray diffraction, scanning electron microscopy, X-ray photoelectron spectra, UV–vis absorption spectroscopy and photoluminescence spectra. A possible mechanism for the growth of $KMnF_3$ microcrystal was proposed.

1. Introduction

The shape is one of the most important factors in determining the structural, physical, and chemical properties of a nanoparticle and an assembled array of the particles [1–5]. Shape-controlled synthesis of nanoparticles has become a recent focus, as different shapes of the particles can introduce electronic, optical, and magnetic properties that are different from those observed in their special counterparts [6,7]. Much effort has been made in the design of rational methods for synthesizing microstructures with various shapes, such as spheres and hollow spheres [8], rods and wires [9], triangle [10], tubes [11] and polyhedral [12], etc., which are interesting for quantum confinement studies and important for potential optical properties applications. To date, the vast majority of all of these interesting compounds are based on transition metals and their associated oxides.

As a class of materials, solid inorganic fluorides possess a number of interesting properties, such as electron-acceptor behavior, a large optical transmission domain, high resistivity, anionic conductivity and photoluminescence [13–18]. Especially, ternary metal fluorides, possessing cubic perovskite structures with a chemical formula of $AMnF_3$ (A = K, NH_4, Rb, Tl, Cs), have generated considerable interest due to their exceptional magnetic, piezoelectric, and photoluminescent properties [19–22]. Recently, well-defined $KMnF_3$ nano- and microcrystals with various morphologies have been reported. For example, cubic-shaped nanoparticles were synthesized by Agnoli et al. using reverse micelle technique [23]; Tang et al. reported the fabrication of acicular-shaped $KMnF_3$ microcrystals via solvothermal treatment [24]; Zhang and co-workers synthesized the microstructures of $KMnF_3$ by an organic monolayer template [25]. However, it is still a challenge to synthesize the materials with various shapes in a facile and environmental friendly way.

Regarding previous work with the microstructures, to the best of our knowledge, $KMnF_3$ microcrystals with hollow structured analogues have not as yet been fabricated. In this work, we have utilized a hydrothermal technique because of its facility of use, its cost-effectiveness, and its relatively mild reaction conditions (low temperature; aqueous solution; reasonably nontoxic reagents) [26], and successfully synthesized $KMnF_3$ microcrystals with three morphologies (polyhedral, sphere and hollow spheres). In the reaction, these microstructures were obtained by just modifying one reaction parameter. This convenient route offers a possible solution to synthesize analogous fluorides with a variety of shapes. The growth mechanism of the microcrystals would be proposed, which was based on a conventional process of Ostwald ripening [27]. Amphiphilic polymer polyethylene glycol was employed for control over the crystal growth and organization.

* Corresponding author at: Division of Nanomaterials and Nanochemistry, Hefei National Laboratory for Physical Sciences at Microscale, Hefei, Anhui 230026, P.R. China. Tel.: +86 551 3601791.
E-mail address: kbtang@ustc.edu.cn (K.B. Tang).

0022-1139/$ – see front matter © 2009 Elsevier B.V. All rights reserved.
doi:10.1016/j.jfluchem.2009.05.018

2. Result and discussion

2.1. Structure and morphologies

Fig. 1a–c shows XRD patterns of as-prepared samples at 120 °C with three PEG strategies, which were carried out without PEG, with PEG1 and PEG2, respectively. Here, PEG1 stands for polyethylene glycol-1000 and PEG2 stands for polyethylene glycol-6000, which possesses higher molecular weight than the former. Three X-ray diffraction patterns are identical and their diffraction peaks can be perfectly indexed to a cubic structure of $KMnF_3$. For instance, all diffraction peaks in Fig. 1a (with lattice constant $a = 4.187$ Å) are in good agreement with the literature values of bulk $KMnF_3$ (JCPDS Card File No. 17-116, space group Pm3m, $a = 4.189$ Å). No characteristic peaks for impurities are observed.

Fig. 2a is a typical SEM image of the sample (Fig. 1a) obtained after aging at 120 °C for 20 h without any PEG, which shows that the product consists of micropolyhedra with 3–6 μm in size. High-magnification SEM image (Fig. 2b) clearly reveals an individual

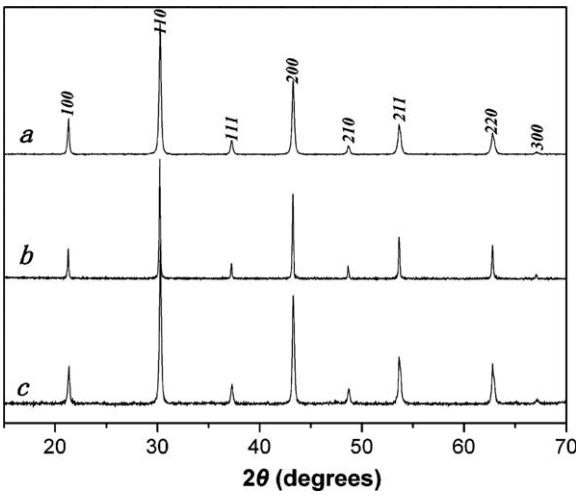

Fig. 1. Shows the XRD patterns of as-prepared $KMnF_3$ microcrystals (a) truncated micropolyhedra; (b) microspheres; (c) hollow microspheres.

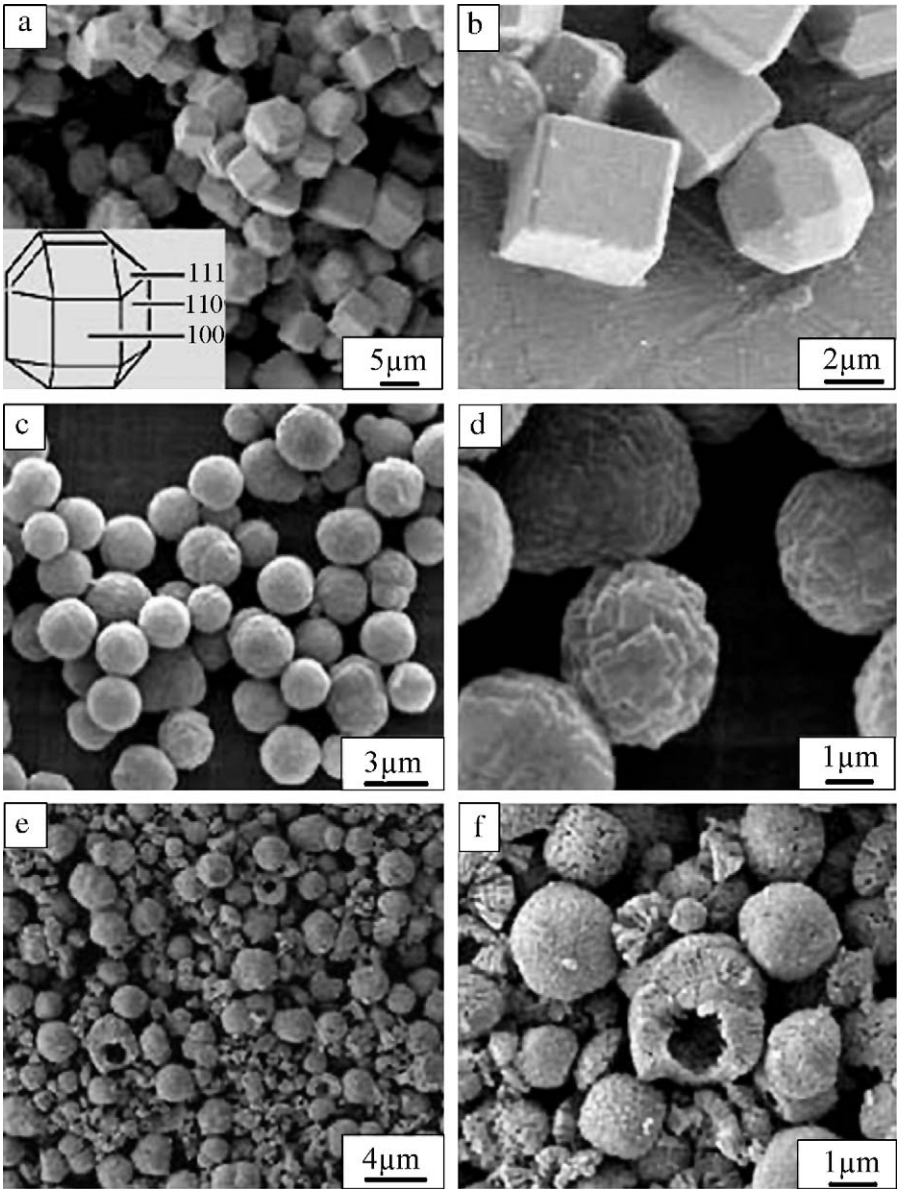

Fig. 2. SEM image of $KMnF_3$ microcrystals formed in various conditions, (a, c, and e) low-magnification images of micropolyhedra, microspheres and hollow microspheres, respectively; (b, d, and f) high-magnification images of micropolyhedra, microspheres and hollow microspheres, respectively.

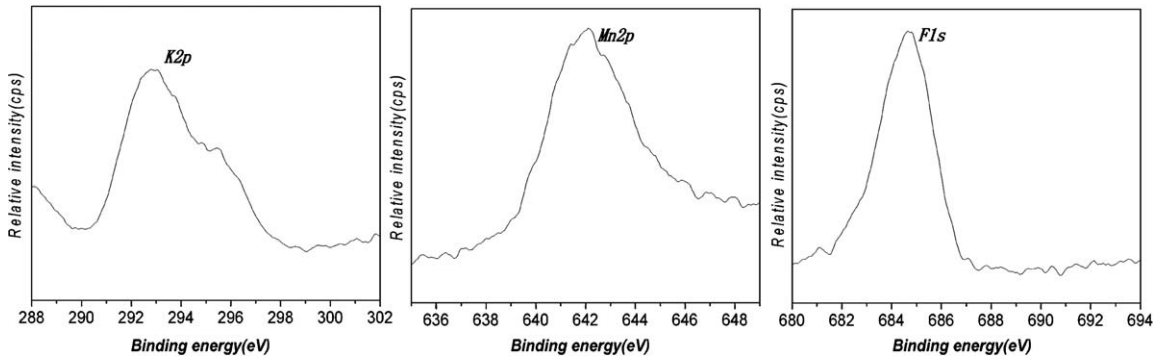

Fig. 3. XPS spectra of as-prepared $KMnF_3$ hollow microspheres.

Table 1
Effects of the PEG on the morphologies of products.

Number	$MnC_4H_6O_4$ (mmol)	$KF{\cdot}2H_2O$ (mmol)	Temp (°C)	Time (h)	Citric acid (mmol)	PEG (mmol)	Products
1	2	6	120	20	2	–	Microcubes and polyhedra
2	2	6	120	20	2	PEG1[a] (2 mmol)	Nanosheet-based solid microspheres
3	2	6	120	20	2	PEG1 (4 mmol)	Incompact spherical grains
4	2	6	120	20	2	PEG1 (8 mmol)	Coarse hollow microspheres
5	2	6	120	20	2	PEG2[b] (0.5 mmol)	Microcubes and microspheres
6	2	6	120	20	2	PEG2 (1 mmol)	Hollow microspheres
7	2	6	120	20	2	PEG2 (3 mmol)	Rough hollow microspheres

[a] PEG1 stands for polyethyleneglycol-1000.
[b] PEG2 for polyethyleneglycol-6000.

cube truncated in certain orientation, which had been defined as "truncated polyhedrons" [28,29]. In the figures, the cubes were truncated by {1 1 0}, {1 1 1} faces and enclosed with crystal face of {1 1 0}, {1 1 1} and {1 0 0}. Some of the cubes with face of {1 1 0} were so heavily truncated that the micropolyhedra were shown more markedly. A proposed schematic illustration for this case is depicted in Fig. 2a (inset). When 2 mmol PEG1 were added to the reaction system as surfactant, homogeneous microspheres were obtained at 120 °C for 20 h as shown in Fig. 2c, which were approximately 3 μm in diameter. Magnified SEM image (Fig. 2d) shows that the spherical structure possessed a rough surface consisting of little sheet-shaped faces. Fig. 2e reveals that the sample was composed of a large quantity of hollow microspheres, which were fabricated using PEG2 as surfactant at 120 °C for 20 h. The diameters of hollow microspheres were in the range of 1–3 μm and inner diameters were in the range of 0.5–1.5 μm. Fig. 2f shows the SEM image of hollow microspheres at a higher magnification that the microstructure had a compact crust, which consisted of nanorods or nanoparticles aligned without any substrate support.

The composition of as-obtained sample with hollow microspheres shape was determined by XPS. A survey spectrum shows the presence of K, Mn, F as well as C, O impurity from the absorption of gaseous molecules. The enlarged spectra performed at K, Mn and F core regions are given in Fig. 3. The binding energy at 292.94 eV and 684.70 eV was corresponding to K 2p and F 1s, which was also consistent with the reported value in the literature [30]. The binding energy of Mn 2p3/2 was found to be 642.09 eV, which was in agreement with that observed in MnF_2 [31]. The analysis to the peak areas indicated that the atomic ratio of K:Mn:F was equal to 0.997:1.077:3. The result reveals that the composition of as-prepared sample was close to the stoichiometry.

2.2. Effect of polyethylene glycol (PEG)

PEG had a significant effect on the morphological development of $KMnF_3$ microstructures. To further investigate the effect, comparative experiments were performed in the case of varying the amount and sorts of PEG and keeping other conditions identical, and the results are displayed in Table 1. When PEG was

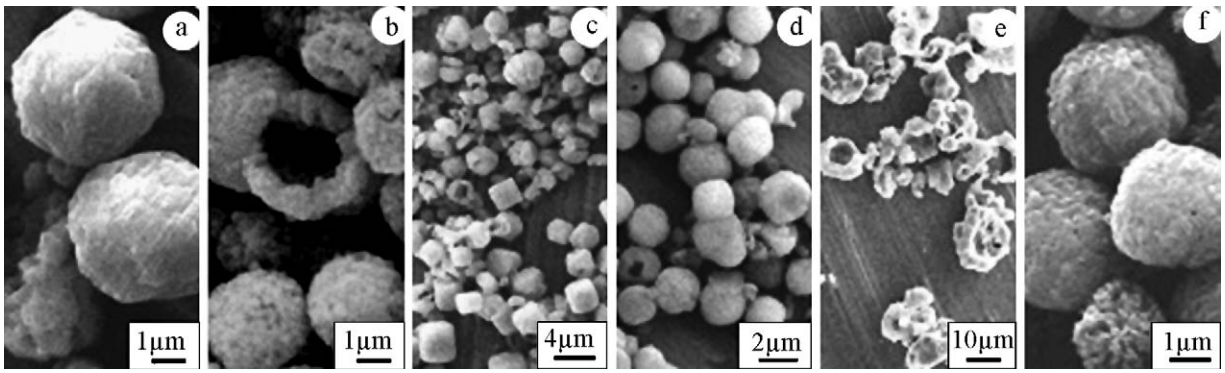

Fig. 4. SEM images of the products under different reaction condition: (a) as-prepared $KMnF_3$ microcrystals used 0.5 mmol PEG1, (b) used 3 mmol PEG1, (c) as-prepared $KMnF_3$ microspheres used 4 mmol PEG2, (d) used 8 mmol PEG2, (e) as-prepared $KMnF_3$ samples without citric acid, and (f) used 1 mmol citric acid.

Table 2
Effects of the dosage of citric acid on the morphologies of products.

Number	$MnC_4H_6O_4$ (mmol)	$KF{\cdot}2H_2O$ (mmol)	Temp (°C)	Time (h)	Citric acid (mmol)	Products
1	2	6	120	20	0	Irregular hollow microcrystals
2	2	6	120	20	1	Inner-loose microspheres
3	2	6	120	20	2	Hollow microspheres
4	2	6	120	20	4	–

absent, micropolyhedra with a range of 3–6 μm in size were obtained. However, when 2 mmol PEG1 was introduced to the hydrothermal system, the morphology of as-obtained samples turned to homogeneous microspheres with nanosheet-like surface (Fig. 2d). When the dosage of PEG1 was increased to 4 mmol, the microspheres with smooth surface and incompact interior could be achieved, and the resulting samples were different from nanosheet-based microspheres (Fig. 4a). Further increasing PEG1 to 8 mmol, the self-assembled hollow microspheres (Fig. 4b) would be obtained, which possessed a rough surface comparing with the microspheres obtained at 1 mmol PEG2 (Fig. 2f). The reaction conditions and results are listed in Table 1 (entry 1–4). When PEG2 was employed instead of PEG1, the morphologies of as-obtained sample had an obvious evolution along with the amount of PEG2. As 0.5 mmol PEG2 was added, the cubes, truncated polyhedra and hollow microspheres coexisted in the system (Fig. 4c). When the dosage of PEG2 was increased to 1 mmol, hollow microspheres can be obtained exclusively. While 3 mmol PEG2 was utilized, hollow microspheres still emerged with slight reduction in size (Fig. 4d). The parameters are listed in Table 1 (entry 5–7), which reveal that PEG2 had a remarkable effect on the formation of unique hollow microspheres in the reaction.

2.3. Effect of citric acid

The influence of citric acid was also investigated in this work. Table 2 summarizes the effect of citric acid on the formation and growth of $KMnF_3$ hollow structure using 1 mmol PEG2 in the reaction. When citric acid was absent, the disorder and irregular hollow microcrystals were observed (Fig. 4e); while 1 mmol citric acid was added, the microspheres with loose structure could be obtained (Fig. 4f). Further increasing the dosage to 2 mmol, hollow microspheres appeared. It could be explained that the citric acid was a suitable complexing agent for the formation of $KMnF_3$ microstructures, and then the weak ligand could incorporate or release metal cations to modulate the rate of crystal growth. Here, taking advantage of the chemical nature, we gave a possible formation process of $KMnF_3$ microcrystals to express the action of citric acid, as follows:

$$3Mn^{2+} + 2R^{3-} \rightarrow 3Mn_3R_2 \quad (1)$$

$$Mn^{2+} + 2F^{-} \rightarrow MnF_2 \quad (2)$$

$$MnF_2 + K^{+} + 3F^{-} \rightarrow KMnF_3 \quad (3)$$

$$Mn_3R_2 + 9KF \rightarrow 3KMnF_3 + 2R^{3-} + 6K^{+} \quad (4)$$

where R represents citric acid, the above reactions were competitive in the reaction system. It means that the shape evolution of $KMnF_3$ microstructure was controlled by the coordination effect between citric acid and Mn^{2+}, in other words, the formation of desired hollow microspheres was closely related to the amount of citric acid. However, when citric acid was increased to 4 mmol, due to lower pH no microcrystals wereobtained in the reaction.

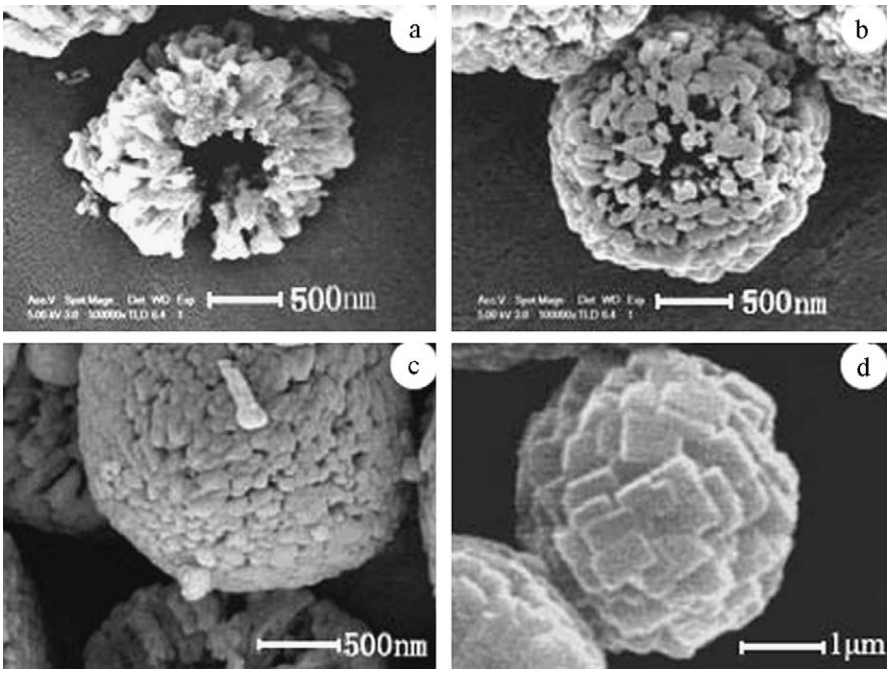

Fig. 5. SEM images of the samples under different evolvement processes: (a)–(c) as-prepared $KMnF_3$ sample by time-dependent experiments used 1 mmol PEG1 at 120 °C for 2 h, 5 h, 20 h, respectively; (d) as-prepared $KMnF_3$ sample used 2 mmol PEG2 at 120 °C for 2 h.

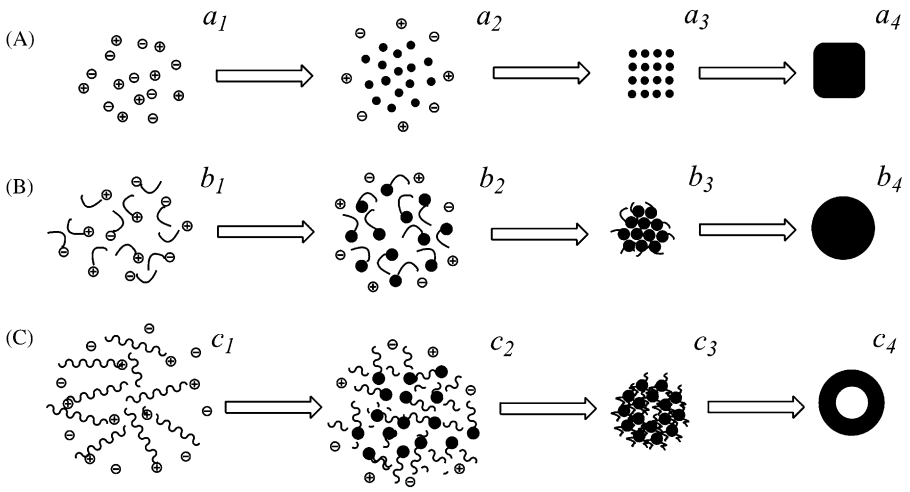

Scheme 1. (A) A schematic formation mechanism of $KMnF_3$ micropolyhedra: (a_1) the initial state of reactant ions without any PEG, (a_2) the process of nucleation, (a_3) the evolution of cube with anisotropic growth and (a_4) formation of cube or polyhedron. (B) A schematic formation mechanism for $KMnF_3$ microspheres: (b_1) the reactant ions adhere to the short-chain of PEG2, (b_2) the formation of colloidal clusters, (b_3) the colloidal clusters dominated by PEG2 evolved into a compact spherical precursor and (b_4) the gathered microspheres with sheet-nanostructure surface. (C) A schematic formation mechanism for $KMnF_3$ hollow microspheres: (c_1) PEG1 long-chains are conglutinated by reactant ions, (c_2) the aggregation of colloids built by ions, (c_3) the formation of loose spherical precursor and (c_4) the formation of $KMnF_3$ hollow microspheres by "Ostwald ripening" process.

2.4. Reaction mechanism

To study the growth mechanism of $KMnF_3$ microstructures, time-dependent experiments were conducted at 120 °C employing PEG2 in the reaction. The SEM images of the three typical hollow microspheres attained at 2 h, 5 h and 20 h of reaction are displayed in Fig. 5a–c respectively, which indicates the evolution of nanoparticle-built hollow microspheres with diameter from 1 μm to 3 μm. Fig. 5d is a magnified SEM image of individual microspheres with a diameter of about 3 μm, which reveals a rough surface of the hierarchical microspheres is constructed from nanosheets. The hierarchical microspheres were fabricated at 120 °C for 20 h using 2 mmol PEG1 as surfactant.

The PEG was hypothesized to play two roles in the reaction: preventing the microspheres from aggregation; controlling the growth speed of different faces by attaching selectively to certain crystal faces [32]. Based on the above results, possible formation mechanisms for various microstructures are proposed here. In the absence of PEG, it was possible that the $KMnF_3$ microcrystals with polyhedral shape were formed spontaneously at 120 °C for 20 h in the reaction due to the anisotropy of crystal growth and its self-limitation character [33] as shown in Scheme 1A. In terms of the formation of microspheres with nanosheet-like surface, PEG1 with chain structure played a key role in the reaction. Initially, a few seeds or colloids were rapidly formed and adsorbed on the short-chain of PEG1. Subsequently, crystal nucleation and growth were restricted by the short-chain adsorption, which can interrupt the self-limitation growth and finally lead to the formation of microspheres to reduce surface energy of microstructures. It is worth noting that the driving force of the short-chain was limited for the formation of well-defined microspheres, and anisotropic crystal growth was still exhibited on the surface of microspheres. Therefore, the nanosheet-like surface can be regarded as the result of using PEG1. This process is depicted in Scheme 1B. In the case of utilizing PEG2, we consider that PEG2 with long-chain had stronger block effects comparing with PEG1. At the beginning, K^+, F^-, Mn^{2+}, acetate and citric acid (R) ions yielded massive $KMnF_3$, MnF_2 or MnR colloids instantaneously in the saturated solution as shown in Eqs. (1)–(4). The nucleation and crystal growth of $KMnF_3$ were confined within the molecular long-chains with a large amount of active oxygen atoms, which possessed an adsorption function. Simultaneously, the nucleation process was also modulated by the coordination effect of citric acid. The initial colloids restricted by the long-chains and modulated by citric acid can assemble to form the loose spherical aggregates in order to minimize their surface energy [34]. With the reaction time prolonged, the loose spherical aggregates which were surrounded by a supersaturated solution grew up gradually. At the same time, the component of aggregates evolved to become $KMnF_3$ as a result of thermodynamic stability. During the ripening process, interior nanocrystallites would dissolve and the outer crust slowly developed to form hollow structures by Kirkendall effect [35,36]. This theory has been widely applied for fabrication of nanoscale hollow structures, which involving an unbalanced counter diffusion through a reaction interface. By localized Ostwald ripening, the following recrystalization of $KMnF_3$ and the fusion of small particles on the exterior crust of microspheres resulted in the smooth surfaces [37–39]. This process is clearly displayed in Fig. 5a–c, which would be continuous until a new equilibrium reaches. A schematic illustration of possible evolutional process for hollow microspheres was given in Scheme 1C.

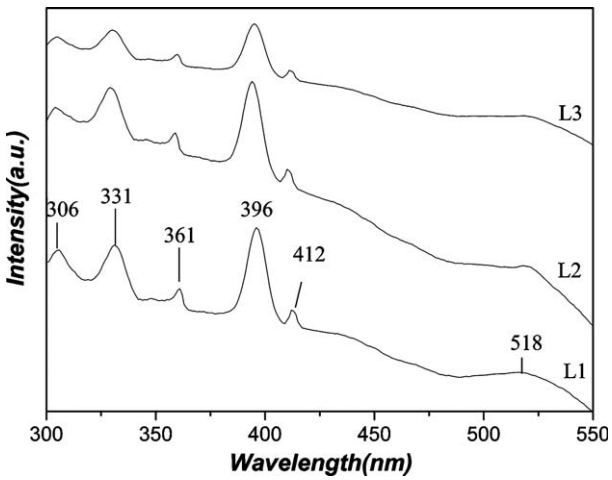

Fig. 6. UV–vis absorption spectra of as-obtained $KMnF_3$ samples, (L1) micropolyhedra, (L2) microspheres, and (L3) hollow microspheres.

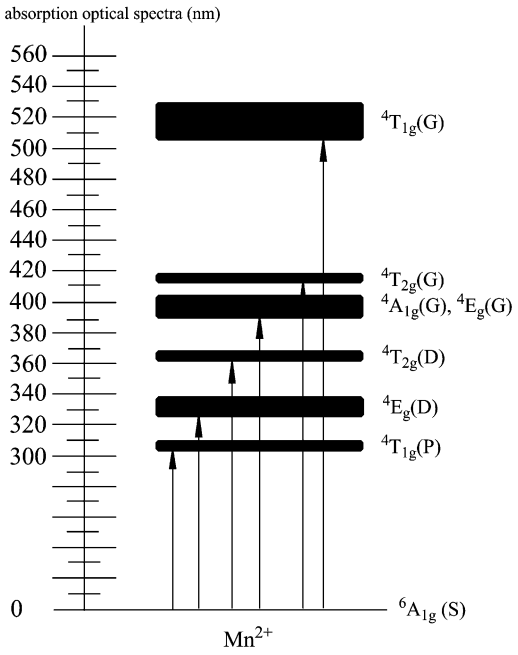

Fig. 7. A schematic diagram of possible electronic transitions corresponding to as-obtained $KMnF_3$ micropolyhedra.

2.5. Optical properties

Fig. 6 shows the typical UV–vis absorption spectra of $KMnF_3$ micropolyhedra (L1), microspheres (L2), and hollow microspheres (L3) with similar profiles, which were in agreement with the pattern previously described by Zhang et al. [40]. For the absorption spectrum of micropolyhedra, bands correspond to Mn^{2+} from the $^6A_{1g}(S)$ ground state to different spin quartet excited states ^4G_g are indicated in L1 of Fig. 6. Featuring two major bands were located at 331 nm [$^4E_g(D)$] and 396 nm [$^4A_{1g}(G)$, $^4E_g(G)$], in addition to three smaller peaks and one wide absorption band centered at 306 nm [$^4T_{1g}(P)$], 361 nm [$^4T_{2g}(D)$], 412 nm [$^4T_{2g}(G)$], and 518 nm [$^4T_{1g}(G)$], respectively. Credible crystal field assignments of all of these bands, corresponding to plausible electronic transitions, are presented in Fig. 7. These transitions were mainly attributed to coupled interactions of the Mn^{2+} ion with the surrounding octahedral array of F^- ions [41,42].

It is well known that light absorption by the material and the migration of the light-induced electrons and holes are key factors for photoluminescence (PL) spectrum, which is relevant to the electronic structure characteristics of the material [43]. Fig. 8 shows the photoluminescence spectra of $KMnF_3$ with micropolyhedral (a), microspheres (b) and hollow microspheres (c) shapes respectively, using excitation wavelength at 373 nm. Overall indigoid emission peaks centered at 400–440 nm were observed, which were similar to the result reported by Goldberg [44]. The corresponding strongest PL emission peaks for $KMnF_3$ micropolyhedra, microspheres and hollow microspheres appeared at 436 nm, 433 nm and 437 nm respectively, secondary peaks at 412 nm, 409 nm, 414 nm and third shoulder peaks centered at 458 nm, 456 nm and 464 nm respectively. Although the major peaks in the emission spectra were identical in these samples, the intensity patterns were different. The weakest luminescence spectrum line belonged to micropolyhedra samples, while the luminescence intensity of hollow microspheres was the most intense at the same measurement conditions. The difference in luminescence properties can be ascribed to the various dimensions, morphologies, and crystal structures. The hollow microspheres possessed more defects from its crystal growth process.

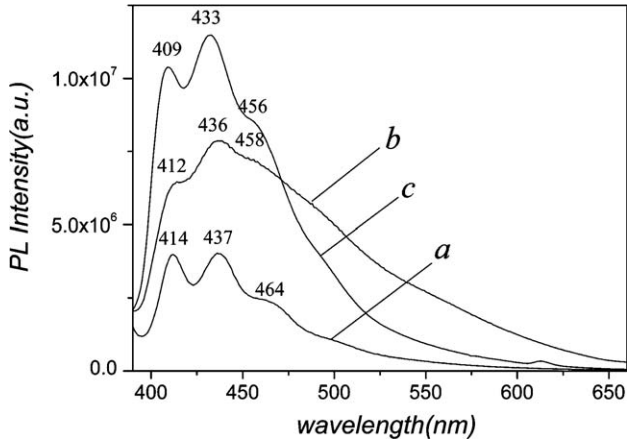

Fig. 8. Room temperature PL spectra of $KMnF_3$ samples: (a) microspheres, (b) micropolyhedra, and (c) hollow microspheres.

3. Conclusion

In summary, micropolyhedra, microspheres and hollow microspheres of cubic $KMnF_3$ have been selectively synthesized through a simple hydrothermal method. The selectivity of polyethylene glycol and the dosage of citric acid have important effects on the development of morphologies. The UV–vis absorption spectra of the as-obtained samples reveal analogous absorption peaks. PL spectra of the as-obtained products show intense emission peaks in range of 400–440 nm. A possible growth mechanism for the hollow microspheres has been tentatively proposed on the basis of the experimental results. The long-chain PEG is used as a well soft template in the synthesis of hollow microspheres. It may promise the manufacture of inorganic materials with unique architecture.

4. Experimental

All chemical reagents (analytical grade), such as polyethylene glycol-1000 (PEG1), polyethylene glycol-6000 (PEG2), manganese acetate ($MnC_4H_6O_4$), potassium fluoride dihydrate ($KF{\cdot}2H_2O$), citric acid ($C_6H_8O_7$) and anhydrous alcohol (C_2H_6O) were purchased from Shanghai Chemical Reagent Ltd. Co. of China, and were used without further purification.

4.1. Samples preparation

A typical synthesis process of $KMnF_3$ hollow microspheres was performed as follows: $C_6H_8O_7$ (2 mmol), PEG2 (1 mmol) and $MnC_4H_6O_4$ (2 mmol) were added into 40 ml deionized water, which were heated up to 60 °C with vigorous stirring. $KF{\cdot}2H_2O$ (6 mmol) was dissolved into another 10 ml deionized water. After quickly mixing two solutions, the as-obtained solution was sealed into a 60-ml Teflon-lined autoclave immediately and maintained at 120 °C for 20 h and then air-cooled to room temperature naturally. The resulting precipitates were collected by centrifugation, washed with distilled water and ethanol for several times, and dried under vacuum at 60 °C for 4 h. Similarly, $KMnF_3$ microspheres and micropolyhedra were synthesized via the same routine, except that just PEG1 instead of PEG2 in the case of microspheres and without any polyethylene glycol (PEG) in the case of micropolyhedra.

4.2. Characterization

The sizes and morphologies of as-obtained samples were characterized by a field emission scanning electron microscope

(JEOL, 7500B) operating at an acceleration voltage of 10 kV and a scanning electron microscopy (X-650 SEM) and X-ray photoelectron spectra were recorded on a VGESCALAB MK II X-ray photoelectron spectrometer, using Mg Kα radiation as the excitation source. Phases' structures were identified in an X-ray diffractometer (XRD, Philips X'pert PRO SUPER) with Cu Kα radiation (λ = 1.54187 Å). Photoluminescence (PL) spectra of samples were obtained from a Hitachi F-4500 fluorescence spectrophotometer at room temperature. UV–visible spectra were recorded on a Shimadzu UV–vis absorbance diode array spectrometer, using 1 cm quartz cuvettes. Prior to the experiment, the as-prepared $KMnF_3$ microcrystals were sonicated in distilled water so as to yield homogeneous dispersions in absolute alcohol.

Acknowledgments

Financial support by the National Natural Science Foundation of China (No. 20371044, 20621061) and the 973 Projects of China is gratefully acknowledged.

References

[1] Z.L. Wang, Adv. Mater. 10 (1998) 13–30.
[2] Z.L. Wang, Z. Dai, S. Sun, Adv. Mater. 12 (2000) 1944–1946.
[3] N.R. Jana, Angew. Chem. Int. Ed. 43 (2004) 1536–1540.
[4] A. Mohraz, D.B. Moler, R.M. Ziff, M.J. Solomon, Phys. Rev. Lett. 92 (1–4) (2004) 155503.
[5] R. Narayanan, M.A. El-Sayed, Nano. Lett. 4 (2004) 1343–1348.
[6] Y. Xia, P. Yang, Y. Sun, Y. Wu, B. Mayer, B. Gates, Y. Yin, F. Kim, H. Yan, Adv. Mater. 15 (2003) 353–389.
[7] X. Peng, J. Thessing, Struct. Bond. 118 (2005) 79–119.
[8] H.X. Li, Z.F. Bian, J. Zhu, D.Q. Zhang, G.S. Li, Y.N. Huo, H. Li, Y.F. Lu, J. Am. Chem. Soc. 129 (2007) 8406–8407.
[9] S.H. Yu, B. Liu, M.S. Mo, J.H. Huang, X.M. Liu, Y.T. Qian, Adv. Funct. Mater. 13 (2003) 639–647.
[10] N. Pinna, K. Weiss, J. Urban, M.P. Pileni, Adv. Mater. 13 (2001) 261–264.
[11] X. Wang, X.M. Sun, D. Yu, B.S. Zou, Y. Li, Adv. Mater. 15 (2003) 1442–1445.
[12] D. Seo, J.C. Park, H. Song, J. Am. Chem. Soc. 128 (2006) 14863–14870.
[13] C.M. Bender, J.M. Burlitch, D. Barber, C. Pollock, Chem. Mater. 12 (2000) 1969–1976.
[14] M. Takashima, S. Yonezawa, J-h. Kim, J. Alloys Compd. 408–412 (2006) 468–473.
[15] G. Ńenert, J. Phys.: Condens. Matter 20 (2008) 335229 (6 pp.).
[16] B.-C. Hong, K. Kawano, J. Alloys Compd. 408 (2006) 838–841.
[17] D. Dambournet, A. Demourgues, C. Martineau, S. Pechev, J. Lhoste, J. Majimel, A. Vimont, J.-C. Lavalley, C. Legein, J.-Y. Buzaré, F. Fayon, A. Tressaud, Chem. Mater. 20 (2008) 1459–1469.
[18] Z. Mazej, J. Fluorine Chem. 125 (2004) 1723–1733.
[19] M.A. Laguna, M.L. Sanjuán, V.M. Orera, J. Rubín, E. Palacios, M.C. Piqué, J. Bartolomé, J.F. Berar, J. Phys.: Condens. Matter 5 (1993) 283–300.
[20] O. Pilla, P.T.C. Freire, V. Lemos, Phys. Rev. B 52 (1995) 177–180.
[21] C. Zhao, S. Feng, R. Xu, C. Shi, J. Ni, Chem. Commun. 10 (1997) 945–946.
[22] J. Kapusta, P. Daniel, A. Ratuszna, Phase Transitions 72 (2000) 165–181.
[23] F. Agnoli, W.L. Zhou, C.J. OConnor, Adv. Mater. 13 (2001) 1697–1699.
[24] Q. Tang, J.M. Shen, W.J. Zhou, Inorg. Chem. Commun. 7 (2004) 283–285.
[25] L.H. Lu, H.S. Wang, H.J. Zhang, J. Colloid Interface Sci. 266 (2003) 115–119.
[26] S. Feng, R. Xu, Acc. Chem. Res. 34 (2001) 239–247.
[27] J.D. Ng, B. Lorber, J. Witz, A. Théobald-Dietrich, D. Kern, R. Giegé, J. Cryst. Growth 168 (1996) 50–62.
[28] M. Petroski, Z.L. Wang, T.C. Green, J. Phys. Chem. B 102 (1998) 3316–3320.
[29] Z.L. Wang, J. Phys. Chem. B 104 (2000) 1153–1175.
[30] J. Chastain, Handbook of X-ray Photoelectron Spectroscopy, Perkin-Elmer, Eden Prairie, MN, USA, 1992.
[31] J.C. Carver, G.K. Schweitzer, T.A. Carlson, J. Chem. Phys. 57 (1972) 973–982.
[32] G.F. Zou, K. Xiong, C.L. Jiang, H. Li, Y. Wang, S.Y. Zhang, Y.T. Qian, Nanotechnology 16 (2005) 1584–1588.
[33] J.S. Wettlaufed, M. Jackson, M. Elbaums, J. Phys. A: Math. Gen. 27 (1994) 5957–5967.
[34] M.S. Mo, J.C. Yu, L.Z. Zhang, Adv. Mater. 17 (2005) 756–760.
[35] Y.G. Sun, Y.N. Xia, Science 298 (2002), 2176–1279.
[36] Y.L. Wang, L. Cai, Y.N. Xia, Adv. Mater. 17 (2005) 473–477.
[37] B. Liu, H.C. Zeng, Small 1 (2005) 566–571.
[38] J.G. Yu, H.T. Guo, S. Mann, Adv. Funct. Mater. 16 (2006) 2035–2041.
[39] H.C. Zeng, J. Phys. Chem. B 108 (2004) 3492–3495.
[40] F.Y.B.M. Zhang, T.-J. Park, S.S. Wong, Adv. Funct. Mater. 18 (2008) 103–112.
[41] P.J. Alonso, V.M. Orera, F. Palacio, R. Alcala, Phys. Stat. Sol. B 109 (1982) K81–K83.
[42] M.V. Iverson, W.A. Sibley, Phys. Rev. B 21 (1980) 2522–2531.
[43] M. Nishida, Phys. Rev. B 66 (1–10) (2002) 125313.
[44] V. Goldberg, D. Pacheco, R. Moncorgé, B. Di Bartolo, J. Lumin. 18 (1979) 143–146.